ORIGINAL RESEARCH

Lung Expression of Human Angiotensin-Converting Enzyme 2 Sensitizes the Mouse to SARS-CoV-2 Infection

Kun Han[1]*, Robert V. Blair[1]*, Naoki Iwanaga[2]*, Fengming Liu[1,3]*, Kasi E. Russell-Lodrigue[1], Zhongnan Qin[1,3], Cecily C. Midkiff[1], Nadia A. Golden[1], Lara A. Doyle-Meyers[1], Mohammad E. Kabir[1,3], Kristin E. Chandler[1], Kellie L. Cutrera[1], Mi Ren[1,3], Christopher J. Monjure[1], Gabrielle Lehmicke[1,3], Tracy Fischer[1,3], Brandon Beddingfield[1], Alanna G. Wanek[2], Angela Birnbaum[1], Nicholas J. Maness[1,3], Chad J. Roy[1,3], Prasun K. Datta[1,3], Jay Rappaport[1,3], Jay K. Kolls[2], and Xuebin Qin[1,3]

[1]Tulane National Primate Research Center, Covington, Louisiana; and [2]Department of Medicine and Department of Pediatrics, Center for Translational Research in Infection and Inflammation, and [3]Department of Immunology and Microbiology, Tulane University School of Medicine, New Orleans, Louisiana

ORCID IDs: 0000-0002-9438-1304 (B.B.); 0000-0002-9332-7891 (N.J.M.); 0000-0002-1710-6974 (C.J.R.); 0000-0001-9875-983X (X.Q.).

Abstract

Preclinical mouse models that recapitulate some characteristics of coronavirus disease (COVID-19) will facilitate focused study of pathogenesis and virus–host responses. Human agniotensin-converting enzyme 2 (hACE2) serves as an entry receptor for severe acute respiratory syndrome coronavirus 2 (SARS-CoV-2) to infect people via binding to envelope spike proteins. Herein we report development and characterization of a rapidly deployable COVID-19 mouse model. C57BL/6J (B6) mice expressing hACE2 in the lung were transduced by oropharyngeal delivery of the recombinant human adenovirus type 5 that expresses hACE2 (Ad5-hACE2). Mice were infected with SARS-CoV-2 at Day 4 after transduction and developed interstitial pneumonia associated with perivascular inflammation, accompanied by significantly higher viral load in lungs at Days 3, 6, and 12 after infection compared with Ad5-empty control group. SARS-CoV-2 was detected in pneumocytes in alveolar septa. Transcriptomic analysis of lungs demonstrated that the infected Ad5-hACE mice had a significant increase in IFN-dependent chemokines $Cxcl9$ and $Cxcl10$, and genes associated with effector T-cell populations including $Cd3 g$, $Cd8a$, and $Gzmb$. Pathway analysis showed that several Kyoto Encyclopedia of Genes and Genomes (KEGG) pathways were enriched in the data set, including cytokine–cytokine receptor interaction, the chemokine signaling pathway, the NOD-like receptor signaling pathway, the measles pathway, and the IL-17 signaling pathway. This response is correlative to clinical response in lungs of patients with COVID-19. These results demonstrate that expression of hACE2 via adenovirus delivery system sensitized the mouse to SARS-CoV-2 infection and resulted in the development of a mild COVID-19 phenotype, highlighting the immune and inflammatory host responses to SARS-CoV-2 infection. This rapidly deployable COVID-19 mouse model is useful for preclinical and pathogenesis studies of COVID-19.

Keywords: SARS-CoV-2; COVID-19; human ACE2; immune responses; mouse model

*These authors contributed equally to this work.

Severe acute respiratory syndrome coronavirus 2 (SARS-CoV-2) continues to spread rapidly, infecting millions of people globally and causing high morbidity and mortality (1, 2). Currently, there are no effective therapeutics or vaccines for prevention and treatment of coronavirus disease (COVID-19) (1, 3, 4). Our current understanding of the pathogenesis of COVID-19 and host interaction with SARS-CoV-2 in humans remains limited and is based primarily upon clinical observations and a few autopsy findings (1). A better understanding of the pathogenesis and host–virus interaction will inform on the development of tractable treatment and prevention strategies for COVID-19 (1). Development of animal models that recapitulate characteristics of human COVID-19 facilitates preclinical studies for

medical product development and our overall understanding of disease pathogenesis. Accordingly, there is an urgency to develop COVID-19 models in nonhuman primates (NHPs) as well as in various small animals and transgenic animals (5).

A recent study demonstrates that ferrets and cats are highly susceptible to SARS-CoV-2 infection, whereas dogs have low susceptibility, and livestock (e.g., pigs, chickens, and ducks) possess essentially no susceptibility (6). SARS-CoV-2 only replicates in the nasal turbinate, soft palate, and tonsils of ferrets, unlike SARS-CoV (the virus that caused pandemic SARS), which replicates in both the upper and lower respiratory tract of ferrets (6). Syrian hamsters, in contrast, develop a mild to moderate clinical syndrome and mild

lung pathology when experimentally infected with SARS-CoV-2 (7). Several laboratories across the world have recently demonstrated a highly reproducible COVID-19 model in the rhesus macaque (*Mucaca mulatta*), with evidence of virus replication and shedding in the mucosa accompanied by mild to moderate clinical signs of disease (5). A recent study using SARS-CoV-2–infected rhesus macaques indicates that SARS-CoV-2 infection protects against reinfection (8), suggesting that immunologic approaches for prevention and treatment of SARS-CoV-2 infection may be possible (8). Although these animal models do not fully recapitulate the severe form of COVID-19, many of the preclinical disease models are being used for assessment and evaluation studies of vaccine and therapeutic
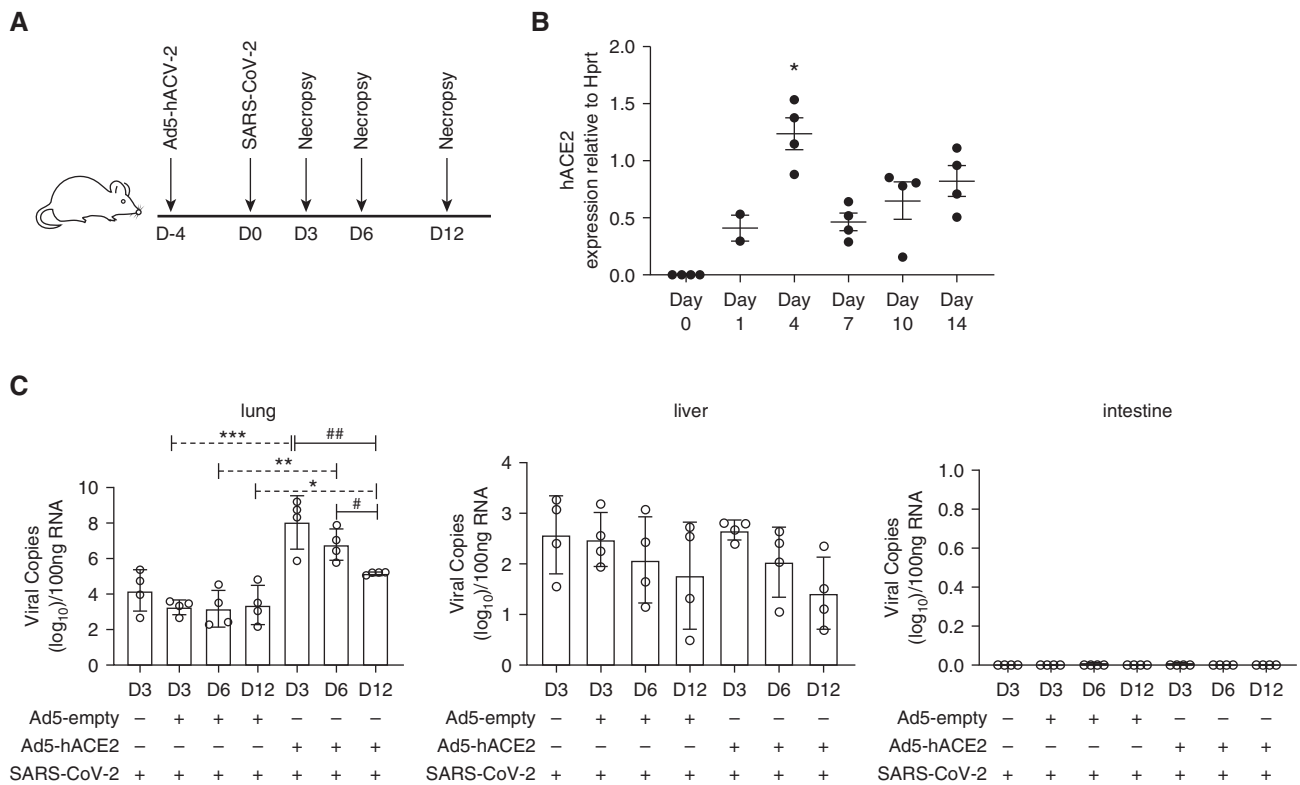
Figure 1. Severe acute respiratory syndrome coronavirus 2 (SARS-CoV-2)-infected Ad5-hACE2 mice had significantly higher viral load in lungs compared with SARS-CoV-2–infected Ad5-empty mice. (*A*) Schematic overview of experimental timeline for establishing and phenotyping Ad5-hACE2 mice (1.5×10^9 PFU, oropharyngeal delivery to B6 mice) infected with SARS-CoV-2 (2×10^5 TCID$_{50}$, IN). (*B*) hACE2 expression in lungs of transduced B6 mice. Ad5-hACE2 vectors were oropharyngeally administered to C57BL/6 mice aged 6 to 8 weeks (1.5×10^9 PFU in 75 μl Dulbecco's modified Eagle medium per mouse) and were killed at 1, 4, 7, 10, and 14 days post transduction (pt). Middle lobes of right lungs were harvested to extract RNA for qRT-PCR at each time point. hACE2 expression was normalized by the housekeeping gene Hprt (internal control). *$P < 0.05$ versus 1, 7, 10, or 14 days pt by one-way ANOVA analysis. (*C*) Viral load after SARS-CoV-2 infection in tissues including lungs, livers, and intestines. *$P < 0.05$, **$P < 0.01$, and ***$P < 0.001$ comparing two groups at the same time intervals by one-way ANOVA analysis. #$P < 0.05$ and ##$P < 0.01$ comparing two time intervals within the group by one-way ANOVA analysis. $n = 4$ for each tissue per group. Ad5 = adenovirus type 5; hACE2 = human angiotensin-converting enzyme 2; Hprt = hypoxanthine-guanine phosphoribosyltransferase; IN = intranasally; PFU = plaque-forming units; TCID$_{50}$ = median tissue culture infectious dose.

candidates and to elucidate basic mechanisms of SARS-CoV-2 infection.

Regardless, small animal models are needed in light of the paucity of NHPs and limited space in biocontainment facilities to perform studies on NHPs in large numbers for COVID-19 therapeutics and vaccines. There is a pressing need to develop an appropriate mouse model because of the potential for high-throughput studies, as well as the accessibility of a large number of molecularly engineered mouse models and the ease of further genetic manipulation (1). Wild-type outbred mouse strains are resistant to SARS-CoV-2 infection (9). Although human agniotensin-converting enzyme 2 (hACE2) serves as an entry receptor for SARS-CoV-2 via binding to its envelope spike (S) proteins, the murine equivalent ACE2 does not provide similar viral entry (2, 10–13). SARS-CoV-2's S protein has a greater affinity to bind to ACE2 than SARS-CoV's S protein (14–17). Transgenic expression of hACE2 in mice sensitizes the mice to SARS-CoV-2 infection, leading to development of a mild COVID-19 phenotype including interstitial pneumonia and elevated cytokines (9, 18). This model is applicable for preclinical and pathogenicity studies of COVID-19. However, to examine the molecular and cellular mechanisms underlying COVID-19, hACE2 must be introduced to various molecularly engineered mouse strains for specific scientific interests. This would be most commonly accomplished via the time-consuming process of breeding multiple generations. Rapidly deployable COVID-19 models would facilitate large-scale *in vivo* screening of preclinical vaccine and therapeutic candidates. Accordingly, we used an adenovirus gene delivery system to express SARS-CoV-2's receptor, hACE2, in the lung (Ad5-hACE2). Lung expression of hACE2 sensitizes the Ad5-hACE2 mouse to SARS-CoV-2 infection. These mice develop moderate to severe interstitial, perivascular inflammation, with evidence of SARS-CoV-2–infected pneumocytes in alveolar septa and a host immune response characteristic of COVID-19. Collectively, this work constitutes the development of a rapidly deployable murine COVID-19 model by viral vector delivery of hACE2 to the lung in an otherwise nonsusceptible mouse strain.

Methods

Mice and Ethics Statement
Additional methodological details are included in the data supplement. Wild-type C57BL/6J mice were housed and bred in the animal facility of Tulane University School of Medicine. The International Care and
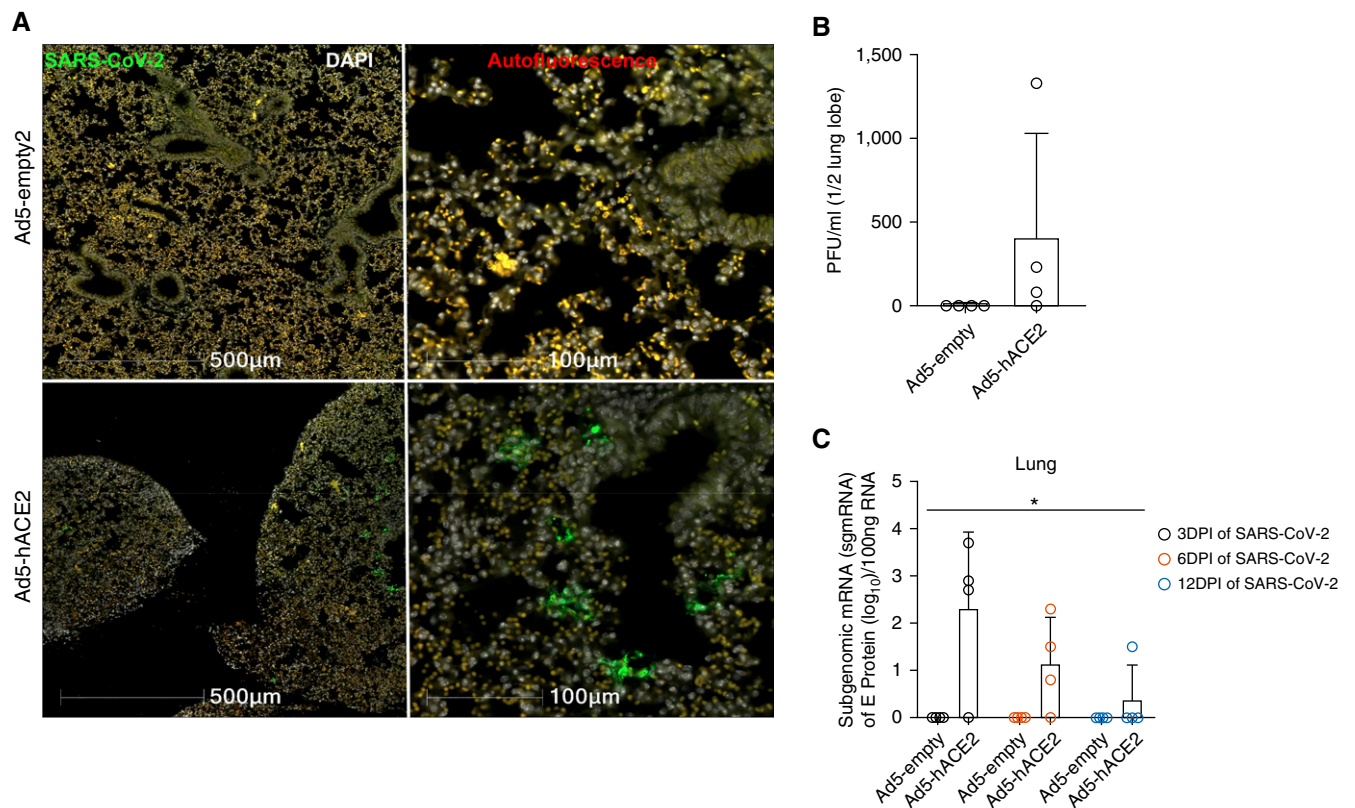
Figure 2. Replicating SARS-CoV-2 was detected in the lung of SARS-CoV-2–infected Ad5-hACE2 but not Ad5-empty mice. (*A*) Immunohistochemistry staining for SARS-CoV-2. Top images show that Ad5-empty mice (control, representative picture for four mice) are negative for SARS-CoV-2 protein. Bottom images show that Ad5-hACE2 mice (representative picture for five mice) have multifocal regions of SARS-CoV-2–positive cells. Scale bars, 100 μm and 500 μm. Green = SARS-CoV-2; White = nuclei/DAPI; Red = empty/autofluorescence. (*B* and *C*) Detection of replicating virus in lungs of mice. Plaque assays at 3 days post infection (dpi) (*B*) and qRT-PCR of viral subgenomic mRNA (sgmRNA) at 3, 6, and 12 dpi (*C*) were used to assess the level of replicating virus in lung tissue. *$P < 0.05$ sgmRNA copies among all groups was measured by two-way ANOVA followed by Bonferroni's multiple comparisons test.

Use Committee of Tulane University reviewed and approved all procedures for this experiment (permit number P0443). The Tulane National Primate Research Center is fully accredited by the Association for Assessment and Accreditation of Laboratory Animal Care.

SARS-CoV-2 Infection

We oropharyngeally transduced the mice with 1.5×10^9 plaque-forming units (PFU) of Ad5-hACE2 or Ad5-empty vectors (Vector Biosystems, Inc.) under Animal Biosafety Level 2 (ABSL2) conditions. hACE2 expression at the transcriptional level in the lungs was determined by qRT-PCR using specific primer pairs for hACE2 and hypoxanthine-guanine phosphoribosyltransferase as the internal control (Cat. No. 4331182; Thermo Fisher). Based on the profiling study, we determined the appropriate day after transduction for infecting the mice with SARS-CoV-2 intranasally by the

ABSL3-trained staff with $5 \times 10^4 - 2 \times 10^5$ median tissue culture infectious dose ($TCID_{50}$) per nostril.

Viral Copy Number Determination

Five microliters of total RNA was added in triplicate to a 0.1-ml fast 96-well optical microtiter plate (Cat. No. 4346906; Thermo Fisher). qRT-PCR reaction (20 μl) was set using TaqPath 1-Step Multiplex Master Mix (Cat. No. A28527; Thermo Fisher) and a premix of forward and reverse primers and a FAM-labeled probe targeting the N1 amplicon of N gene (2019-nCoV RUO Kit, Cat. No. 10006713; IDT-DNA) of SARS-CoV-2 (accession MN908947), following the manufacturer's instructions. Viral load was calculated by the linear regression function by Cq values acquired from 2019 nCoV qRT-PCR Probe Assays (27805681; Integrated DNA Technologies). The viral copy numbers from the lung samples are represented as copies/100 ng of RNA. Subgenomic mRNA (sgmRNA) encoding

the E gene was quantified using a published assay (19).

Statistics

Data are expressed as mean ± SEM. To compare values obtained from multiple groups over time, two-way ANOVA (Kruskal-Wallis test) was used. To compare values obtained from two groups, two-tailed unpaired student's two-tailed unpaired Student's t test was performed. Statistical significance was taken at the $P < 0.05$ level.

Results

Lung Expression of Human ACE2 Renders the Mouse Sensitive to SARS-CoV-2 Infection

To transduce the expression of hACE2 in the mouse lung, we administered adenovirus 5–expressing hACE2 (Ad5-hACE2) oropharyngeally to wild-type B6 mice (Figure 1A). hACE2 was detected in the
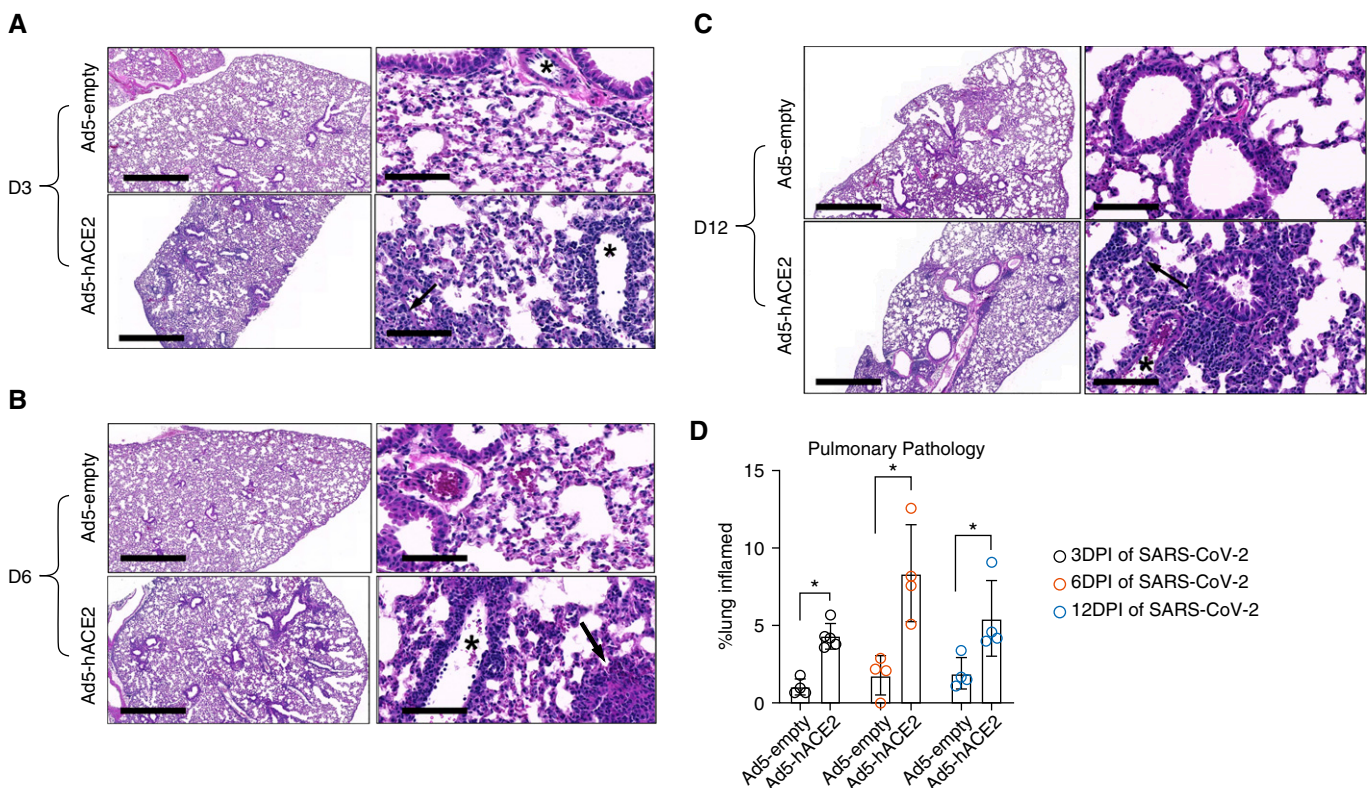
Figure 3. SARS-CoV-2–infected Ad5-hACE2 mice developed more severe interstitial pneumonia associated with perivascular inflammation in the lungs than SARS-CoV-2–infected Ad5-empty mice. (A–C) Hematoxylin and eosin staining shows histological changes in the lungs of Ad5-hACE2 and Ad5-empty mice infected by SARS-CoV-2 at 3 (A), 6 (B), and 12 dpi (C). Asterisks denote an inflamed vessel. The arrow points to an area of interstitial inflammation. Scale bars, 1 mm (left) and 100 μm (right). (D) Quantification of pulmonary pathology. The percentage of lung that is infiltrated by inflammatory cells was quantified with a deep learning algorithm. There was a significant increase in inflammation in SARS-CoV-2–infected mice at 3, 6, and 12 dpi in mice transfected with Ad5-hACE2 compared with those that received an Ad5-empty vector. *$P < 0.05$ with Mann-Whitney U test.

lung of Ad5-hACE2 mice at transcriptional levels at 1 day post transduction (pt), peaked at 4 days pt, and then declined and maintained a level at 7, 10, and 14 days pt comparable with the level at 1 day pt, indicating that hACE2 starts to maintain stable levels after 7 days pt (Figure 1B). We infected mice at 4 days pt with SARS-CoV-2 (intranasal delivery of 2×10^5 $TCID_{50}$ per mouse) (Figure 1A). Infected Ad5-hACE2 mice had several log-fold higher SARS-CoV-2 loads in the lungs than Ad5-empty mice at 3, 6, and 12 days post infection (dpi) (Figures 1C and E1 in the data supplement). In the infected Ad5-hACE2 mice, the viral load in the lung reached the highest level at 3 dpi and gradually declined from 3 to 12 dpi to a level that was still significantly higher than infected

Ad5-empty mice (Figure 1C). We did not detect any significant difference in viral loads in the livers and intestines of infected Ad5-hACE2 and Ad5-empty mice. Furthermore, using immunohistochemistry, we detected SARS-CoV-2 virus in the lungs of SARS-CoV-2–infected Ad5-hACE2 but not Ad5-empty mice at 3 dpi (Figure 2A). Similarly, infectious virus was isolated from lungs of three of four Ad5-hACE2 but not Ad5-empty mice killed at 3 dpi assessed by plaque assay (titer ranging from 0 to 1,332 PFU/ml in the Ad5-hACE2 mice) (Figure 2B) whereas the sgmRNA encoding the viral E protein was likewise amplified from lungs of three of four Ad5-hACE2 (ranging from 0 to 3.7 log viral RNA copies/100 ng of total RNA) but not Ad5-empty mice with the level of sgmRNA

associated strongly with the PFU titer (Figure 2C). We also detected sgmRNA from lungs of three of four and one of four Ad5-hACE2 but not Ad5-empty mice at 6 and 12 dpi, respectively (Figure 2C). Unexpectedly, live virus was not detected in lung from one Ad5-hACE2 mouse at 3 dpi and sgmRNA was not detected in lungs from one Ad5-hACE2 mouse at 3 and 6 dpi. These data could be due to inherent variability associated with detecting live virus or viral RNA in a solid tissue sample, suboptimal storage of the samples, or another reason. Nonetheless, these results indicate that lung expression of hACE2 sensitizes the mouse to SARS-CoV-2 infection.

Infected Ad5-hACE2 mice developed more severe lesions in lungs than infected
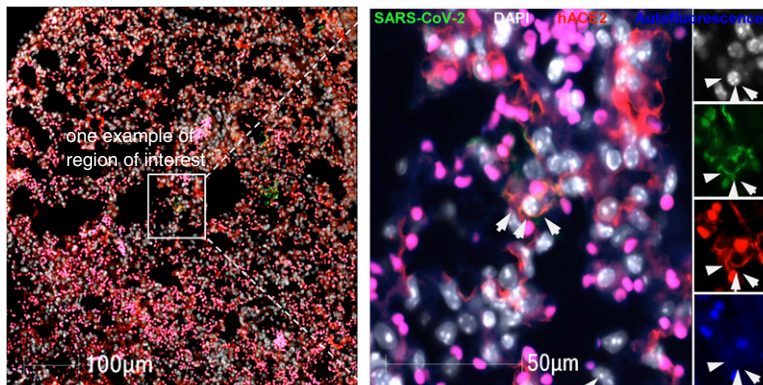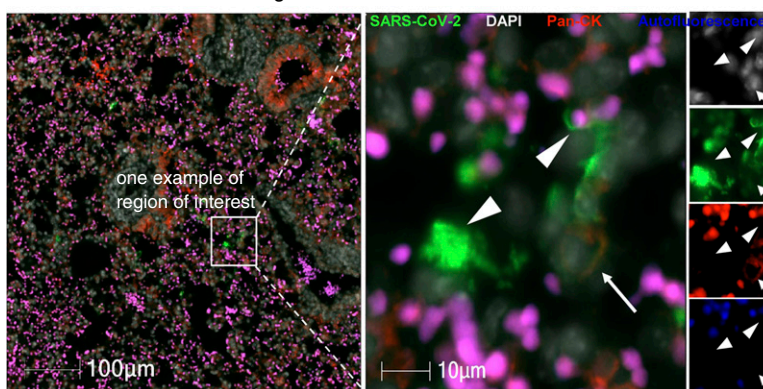
Figure 4. Costaining SARS-CoV-2 with hACE2 or *Pan-cytokeratin* (Pan-CK) in lung of SARS-CoV-2–infected mice at 3 dpi. (*A*) Fluorescent immunohistochemistry (FIHC) for hACE2 with SARS-CoV-2. (*B*) FIHC for Pan-CK with SARS-CoV-2. Left panel: Low-power magnification that shows a region of positive virus staining. Middle panel: Higher magnification that shows a representative image of costaining (arrows) and lack of costaining (arrowheads) of hACE2 or Pan-CK (red) with SARS-CoV-2 (green). Right panel: Quantification of the number of SARS-CoV-2–positive regions in the lung (white bar correlated to the left *y*-axis), and the percentage that exhibited costaining with hACE2 (or Pan-CK) (gray bar correlated with the right *y*-axis) within all regions ($n = 8$). Scale bars, 10 μm, 50 μm, and 100 μm. Green: SARS-CoV-2. White: DAPI. Red: hACE2 or Pan-CK. Blue: autofluorescence.

Ad5-empty mice at 3, 6, and 12 days after SARS-CoV-2 infection, namely, interstitial and perivascular inflammation associated with infiltration of large numbers of lymphocytes and macrophages (Figures 3A, 3B, and 3C). Lesion development began at 3 dpi, reached peak level at 6 dpi, and partially resolved at 12 dpi (Figure 3D). We found no histological changes in other organs including liver, kidney, intestine, heart, and brain in Ad5-hACE2 and Ad5-empty mice (Figure E2). There were no significant differences in body weight, blood cell counts, or serum chemical measurements between the two groups (Figures E3 and E4). Of note, the Ad5-hACE2 mice infected with three different doses of SARS-CoV-2 (5×10^4, 1×10^5, or 2×10^5, $TCID_{50}$) also developed mild or moderate interstitial and perivascular inflammation in the lungs (Figure E5). Together, these results indicate that lung expression of hACE2 sensitized the mouse to SARS-CoV-2 infection and resulted in the development of a mild COVID-19 phenotype.

SARS-CoV-2 Colocalizes with Pan-CK^{+} Type 1 and Type 2 Pneumocytes but Not CD206^{+} Macrophages or CD3^{+} T Cells

SARS-CoV-2 mainly targets and infects ACE2-expressing type 1 and 2 pneumocytes in patients, causing severe clinical disease and lung histological changes (1, 20, 21). To further characterize the COVID-19 mouse model, we used fluorescent immunohistochemistry to colocalize SARS-CoV-2 with hACE2 or with multiple cellular phenotypic markers, including CD206 for macrophages, CD3 for T cells, and *Pan-cytokeratin* (Pan-CK) for pneumocytes (Figures 4 and E6). We found a large number of hACE2-positive cells in the lung of SARS-CoV-2–infected Ad5-hACE2 mice at 3 dpi (Figure 4A, left panel). Interestingly, among the total SARS-CoV-2–positive regions (i.e., a group of positive cells), 75% exhibited colocalization with hACE2-positive cells (Figure 4A). The fact that the overlap was not 100% could be attributed to the downregulation of hACE2 to undetectable levels owing to the internalization of SARS-CoV-2 with its receptor hACE2 during infection (1), a notion that warrants further investigation.

We also detected T cells and macrophages in the lung of the Ad5-hACE2 but not Ad5-empty mice infected with

SARS-CoV-2 at 3 dpi, resulting in moderate to severe interstitial and perivascular inflammation. However, no staining of T cells or macrophages with SARS-CoV-2 was noted (Figure E6). Interestingly, we found SARS-CoV-2–positive pneumocytes in alveolar septa with Pan-CK[+] (Figure 4B). Among the total SARS-CoV-2–positive regions, we detected ~25% that were positive and colocalized with Pan-CK–positive cells (Figure 4B, left). Extensive spike RNA was detected by RNAscope in the interstitial areas of infected Ad5-hACE2 at 3 dpi but not Ad5-empty mice at 3 and 6 dpi (Figure 5A). Specific RNA probes for spike RNA and mouse Hopx (homeobox only protein x) were used to detect SARS-CoV-2 RNA in pneumocytes (22, 23) (Figure 5B). Consistently, we also found that there were SARS-CoV-2-S RNA and Hopx RNA double-positive cells and SARS-CoV-2 RNA-positive cells in the infected Ad5-hACE2 mice at 3 dpi (Figure 5B). Taken together, these results indicate that SARS-CoV-2 can infect pneumocytes, which may contribute to the development of the interstitial and perivascular inflammation seen in SARS-CoV-2–infected Ad5-hACE2 mice. This finding is consistent

with the current view that the majority of SARS-CoV-2–infected cells are pneumocytes (1, 20). However, given that only 25% of the SARS-CoV-2–infected regions were composed of pneumocytes, our data also indicate that other cell types may be susceptible to infection.

Transcriptomic Analysis of Lung Obtained from SARS-CoV-2–infected Ad5-hACE2 and Ad5-Empty Mice

RNAseq analysis was performed at 3 dpi in Ad5-hACE2 and Ad5-empty mice. We observed a significant increase in IFN-dependent chemokine *Cxcl9* (Figure 6) in Ad5-hACE2 mice. Consistently, RNAscope studies also exhibited an upregulated *Cxcl9* at 3 dpi in lungs of infected Ad5-hACE2 mice (Figure 5A). We also observed an increase in *Cd3 g, Cd8a,* and *Gzmb.* This is similar to what has been reported in human BAL samples with distinct populations of CD4^{+}, CD8^{+}, and B cells (24) as well as the presence of Tfh cells in blood of recovered subjects (25). We observed induction of genes associated with effector T-cell populations including *Il21* and *Il21r* (Figure 6) but did not pass the false discovery rate (FDR) filter. Pathway analysis showed that several Kyoto
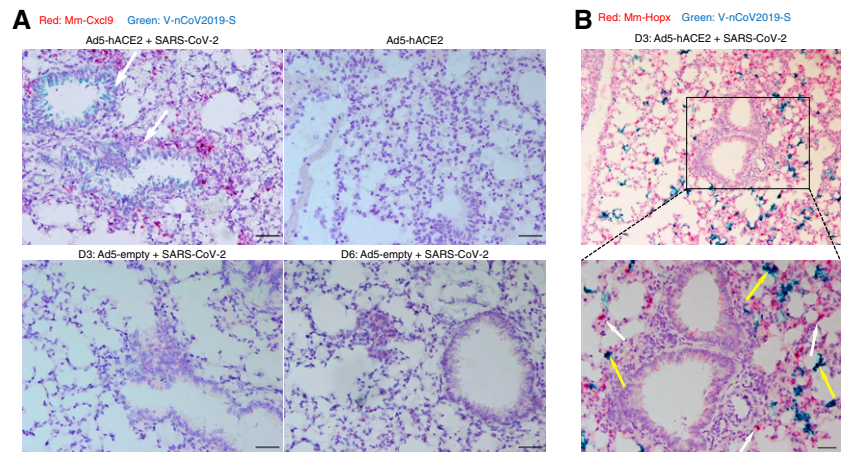
Figure 5. RNAscope detection of either colocalization of spike RNA with *Cxcl9* or colocalization of spike RNA with lung epithelial transcriptional factor, *Hopx* RNA in the pulmonary cells of the infected mice. (*A*) Costaining of spike RNA with *Cxcl9*, a chemokine responsible for type I immunity. Representative image (*n* = 3–4) in *A*, upper panel, shows staining of the spike RNA in the bronchial epithelial cells of the Ad5-hACE2 mice only with SARS-CoV-2 infection at 3 dpi. The lower panel shows no staining of the spike RNA in the lung of the infected Ad5-empty mice at 3 and 6 dpi. *Cxcl9* was only detected in D3 SARS-CoV-2–infected Ad5-hACE2 mice. Red signal: *Mm-Cxcl9*. Green signal: *V-nCoV2019-S*. (*B*) Costaining of spike RNA with *Hopx*. SARS-CoV-2 was detected in interstitial area. Uninfected pneumocytes showed normal red, pointed out by white arrows. Infected pneumocytes showed a darker color caused by the combination of green and red, pointed out by yellow arrows. Red signal: *Mm-Hopx*. Green signal: *V-nCoV2019-S*. Scale bars, 100 μm.

Encyclopedia of Genes and Genomes (KEGG) pathways were enriched in the data set (Tables 1 and E1), including cytokine–cytokine receptor interaction, the chemokine signaling pathway, the NOD-like receptor signaling pathway, the measles pathway, and the IL-17 signaling pathway.

Immune Response to SARS-CoV-2 Infection in Ad5-hACE2 Mice

Clinical studies (26) indicate that from the onset of COVID-19 pneumonia, the levels of T and B lymphocytes gradually increase during treatment in nonsevere patients to levels significantly higher than patients with severe disease. There are no reports yet exploring peripheral immune cell responses in mouse models. The peripheral immune response to SARS-CoV-2 infections was explored in this study by monitoring immune cells in circulation. SARS-CoV-2–infected Ad5-hACE2 mice had significantly higher levels of peripheral $CD4^+$ and $CD8^+$ T cells and B cells than SARS-CoV-2–infected Ad5-empty mice at 6 and 12 dpi (Figure E7).

Discussion

In this paper, we report the generation and characterization of a rapidly deployable COVID-19 mouse model. The lung expression of hACE2 via oropharyngeal delivery of Ad5-hACE2 to wild-type mice sensitizes the mouse to SARS-CoV-2 infection. SARS-CoV-2–infected Ad5-hACE2 mice had several log-fold higher SARS-CoV-2 viral load in the lung than the infected Ad5-empty mice. The infected Ad5-hACE2 mice developed mild COVID-19 with moderate to severe interstitial and perivascular inflammation in the lungs, without lethality or loss of body weight. Of note, we also detected a low SARS-CoV-2 viral load level (from 3 to 12 dpi) in the lungs of the infected Ad5-empty mice by qRT-PCR. However, infectious virus as measured by plaque assay was detected in lungs of Ad5-hACE2 but not Ad5-empty mice killed at Day 3 after infection. Similarly, viral sgmRNA was detected predominantly in Ad5-hACE2 mice at Day 3 and 6 after infection, suggesting that

the presence of viral sgmRNA is an adequate surrogate assay for detection of replicating virus. Furthermore, fluorescent immunohistochemistry did not find any SARS-CoV-2–positive regions in the lungs of the infected Ad5-empty mice. In addition, our RNAscope results did not detect extensive SARS-CoV-2 RNA in the lungs of the infected Ad5-empty mice at 3 and 6 dpi (Figure 5A, lower panel). These results indicate that SARS-CoV-2 in the Ad5-empty mice did not infect pneumocytes or cause interstitial pneumonia owing to lack of the hACE2 receptor in Ad5-empty mice for viral replication, which further supports the role of hACE2 in facilitating SARS-CoV-2 infection in transduced mice. Two recently published reports demonstrated that hACE2-transduced mice in two different mouse strains, including B6 and BALB/c generated by similar approaches, were productively infected with SARS-CoV-2, and this resulted in high viral titers in the lung, corresponding pathology, and weight loss (27, 28). Furthermore, using this approach, they demonstrated that 1) type I IFN, T cells, and STAT1 signaling are critical for viral clearance and disease resolution in these mice (28) and 2) passive transfer of a neutralizing monoclonal antibody reduced viral burden in the lung and mitigated COVID-19 phenotypes in the infected mice (27). Our results reported here further confirm this approach to generate a rapidly deployable COVID-19 model. Of note, we did not observe the same clinical changes (weight loss) in our transduced mice. This may be attributed to the different Ad5-hACE2 titer resulting in different hACE2 levels in the transduced mice, different SARS-CoV-2 viral titer, the different strains of mice, or different environmental conditions in the animal facility causing a difference in microbiome (known to differ between animal houses) important in dictating resistance to COVID19. This difference notwithstanding, our results further confirm recently reported findings that lung expression of hACE2 sensitizes mice to SARS-CoV-2 infection. The lung histological changes in these rapidly deployable COVID-19 models seen by us and others (27, 28) are comparable with recently published observations in SARS-CoV-2–infected hACE2 transgenic mice (9, 18). Transgenic expression of hACE2 in mice also sensitizes them to SARS-CoV-2
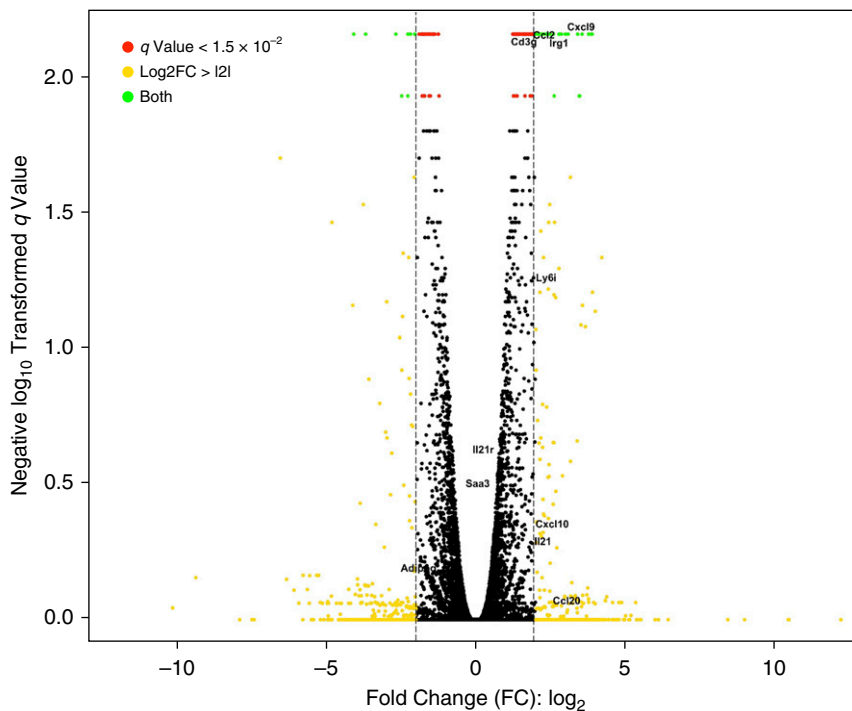
Figure 6. Transcriptomic analysis of whole lung of SARS-CoV-2–infected Ad5-hACE2 and Ad5-empty mice. A volcano plot of differentially expressed genes in Ad5-hACE2 mice infected with SARS-CoV-2 ($n = 3$) compared with infected Ad5-empty mice ($n = 3$) at 3 dpi is shown. The x-axis coordinate was log2 (fold change) and the y-axis coordinate was negative log10 transformed q value. Green dots represent up- or downregulated genes of significant expression. Red dots represent genes of significant expression but less up- or downregulated. Black and yellow dots were genes of nonsignificantly different expression.

Table 1. KEGG Pathways Enriched in SARS-CoV-2–infected Ad5-hACE2 Mice

Pathway	P value
Cytokine–cytokine receptor interaction	2.3×10^{-6}
Chemokine signaling pathway	2.9×10^{-6}
NOD-like receptor signaling pathway	1.8×10^{-5}
Primary immunodeficiency	5.7×10^{-5}
Staphylococcus aureus infection	9.4×10^{-5}
Measles	0.00025
Osteoclast differentiation	0.00031
IL-17 signaling pathway	0.00062
T-cell receptor signaling pathway	0.00066
Changes disease (American trypanosomiasis)	0.00075
Hematopoietic cell lineage	0.00080
Toll-like receptor signaling pathway	0.00085
PD-L1 expression and PD-1 checkpoint pathway in cancer	0.00206
Influenza A	0.00027
Systemic lupus erythematosus	0.00253
Amphetamine addiction	0.00309
Circadian entrainment	0.00393
Cytosolic DNA-sensing pathway	0.00469
Th1 and Th2 cell differentiation	0.00591
Th17 cell differentiation	0.00838
Estrogen signaling pathway	0.00839
Tuberculosis	0.00845
Human cytomegalovirus infection	0.00899
Leishmaniasis	0.01052
Fluid shear stress and atherosclerosis	0.01156
Prion diseases	0.01219
Pertussis	0.01410
Pathways in cancer	0.01483
Hepatitis C	0.01516
Aldosterone synthesis and secretion	0.01531
Apoptosis	0.01557
Melanogenesis	0.01618
Alcoholism	0.01827
Signaling pathways regulating pluripotency of stem cells	0.01835
Phototransduction	0.02948
TGF-β signaling pathway	0.03186
CAMs	0.03360
Rheumatoid arthritis	0.03536
Mineral absorption	0.03565
Salivary secretion	0.03688
Gastric acid secretion	0.03695
Alzheimer disease	0.04455
B-cell receptor signaling pathway	0.04922

Definition of abbreviations: Ad5 = adenovirus type 5; CAMs = cell adhesion molecules; hACE2 = human angiotensin-converting enzyme 2; KEGG = Kyoto Encyclopedia of Genes and Genomes; NOD-like = nucleotide-binding oligomerization domain-like; PD-1 = programmed cell death protein 1; PD-L1 = programmed death-ligand 1; SARS-CoV-2 = severe acute respiratory syndrome coronavirus 2; TGF-β = transforming growth factor β; Th1 = T-helper cell type 1; Th2 = T-helper cell type 2; Th17 = T-helper cell type 17.

infection, leading to a mild COVID-19 phenotype, interstitial pneumonia, and elevated cytokines (9, 18).

We further characterized the phenotype of the cells infected by SARS-CoV-2 in the lung, an aspect of infection that has not been investigated previously in any animal models (6, 8, 9, 18, 27). Our costaining and RNAscope results indicate that SARS-CoV-2 infects pneumocytes, which contributes to the development of interstitial pneumonia seen in the lungs of SARS-CoV-2–infected Ad5-hACE2 mice. The finding of SARS-CoV-2–infected pneumocytes directly supports the current view that SARS-CoV-2 mainly targets and infects pneumocytes (1, 20, 21). In addition, our model developed not only moderate to severe interstitial but also perivascular inflammation in alveolar septa. This distinctive vascular injury in the lung has been noted but not characterized in a SARS-CoV-2–infected hACE2 transgenic line (18). This finding is consistent with a recent clinical observation (29) showing that the histologic pattern of patients that died from severe COVID-19 included diffuse alveolar damage with perivascular T-cell infiltration in the peripheral lung (29). The affected lung also showed distinctive vascular features, consisting of severe endothelial injury associated with the presence of intracellular virus and disrupted cell membranes (29).

We report transcriptomic changes in the lung that are correlative with what has been reported with human COVID-19 (24) using scRNAseq. We observed evidence of a robust adaptive immune response with expression of *Cd3g, Cd8a, Gzmb,* and markers of effector T cells (*Il21* and *Il21r*), which have all been reported in patients with COVID-19 (24, 30). Supportively, a large-scale single-cell transcriptomic analysis of viral antigen-reactive CD4$^+$ T cells from 32 patients with COVID-19 showed increased proportions of cytotoxic follicular helper cells and cytotoxic T-helper cells (CD4-CTLs) responding to SARS-CoV-2 in patients with severe disease compared with those with mild disease (31). This model may be a useful tool to dissect the role of these cells in the pathogenesis of COVID-19 using our recently established cell ablation models (32–36).

SARS-CoV-2–infected mice had significantly higher T and B cells in the circulation only at 6 and 12 dpi. This was also associated with increased infiltration of lymphocytes into the lungs. Previous clinical studies indicate that from the onset of COVID-19 pneumonia, the level of T lymphocytes gradually increased during the disease course in nonsevere patients and was always significantly higher than patients with severe illness (26). The time of recovery of T-lymphocyte count was approximately consistent with the clinical course (26). This indicates that the robust adaptive immune response stimulated by SARS-CoV-2 may contribute to disease recovery or progression, which warrants further investigation.

Conclusions
A great strength of using the adenovirus delivery system for expressing hACE2 in mice is the immediate capability of conducting pathogenesis and preclinical studies in any given genetic background and molecularly engineered mouse strains. Specifically, this rapidly deployable

COVID-19 mouse model recapitulates numerous important characteristics of COVID-19 disease to inform preclinical studies (37). Indeed, passive transfer of a neutralizing monoclonal antibody has been documented to reduce viral burden in the lung and mitigate inflammation and weight loss using a similar model (27). Ad5-hACE2–transduced mice also enabled rapid assessments of a vaccine candidate, of human convalescent plasma, and of antiviral therapies (poly I:C and remdesivir) (9). Our results showed that after SARS-CoV-2 infection, the Ad5-hACE2 mice developed histological changes and immune infiltration associated with the viral load in the lung within 6 dpi. This disease course is comparable with previously published mouse COVID-19 models (6, 8, 9, 27). Based on these reproducible results, we suggest that this rapidly deployable model can serve as an *in vivo* screening tool for the development of vaccines and therapeutics. Therefore, this model can be used to measure the viral load and subgenomic RNA via RT-PCR, analyze the virus in the lung with immunochemistry, and monitor histological changes and immune cell infiltration in the lung for determining the efficacy of the candidate vaccines and therapeutics. This rapidly deployable COVID-19 model should be useful for studying SARS-CoV-2–induced lung pathology. However, owing to their local and temporally limited expression of hACE2, it is conceivable that while considering and designing experiments to explore the impact of SARS-2 infection on other organs such as heart, brain, and kidney, the Ad5-hACE2 mice would be less favorable than transgenic hACE2 mice (9). Clearly, there is an urgent need for such a small rodent model for high-throughput studies testing therapeutic interventions and vaccines for SARS-CoV-2 infection of the lung. ∎

References

1. Datta PK, Liu F, Fischer T, Rappaport J, Qin X. SARS-CoV-2 pandemic and research gaps: understanding SARS-CoV-2 interaction with the ACE2 receptor and implications for therapy. *Theranostics* 2020;10: 7448–7464.
2. South AM, Diz DI, Chappell MC. COVID-19, ACE2, and the cardiovascular consequences. *Am J Physiol Heart Circ Physiol* 2020;318:H1084–H1090.
3. Hedrick TL, Murray BP, Hagan RS, Mock JR. COVID-19: clean up on IL-6. *Am J Respir Cell Mol Biol* 2020;63:541–543.
4. Evans SE, Tseng CK, Scott BL, Höök AM, Dickey BF. Inducible epithelial resistance against coronavirus pneumonia in mice. *Am J Respir Cell Mol Biol* 2020;63:540–541.
5. Callaway E. Labs rush to study coronavirus in transgenic animals: some are in short supply. *Nature* 2020;579:183.
6. Shi J, Wen Z, Zhong G, Yang H, Wang C, Huang B, *et al*. Susceptibility of ferrets, cats, dogs, and other domesticated animals to SARS-coronavirus 2. *Science* 2020;368:1016–1020.
7. Chan JFW, Zhang AJ, Yuan S, Poon VKM, Chan CCS, Lee ACY, *et al*. Simulation of the clinical and pathological manifestations of Coronavirus Disease 2019 (COVID-19) in golden Syrian hamster model: implications for disease pathogenesis and transmissibility. *Clin Infect Dis* [online ahead of print] 26 Mar 2020; DOI: 10.1093/cid/ciaa325.
8. Chandrashekar A, Liu J, Martinot AJ, McMahan K, Mercado NB, Peter L, *et al*. SARS-CoV-2 infection protects against rechallenge in rhesus macaques. *Science* 2020;369:812–817.
9. Bao L, Deng W, Huang B, Gao H, Liu J, Ren L, *et al*. The pathogenicity of SARS-CoV-2 in hACE2 transgenic mice. *Nature* 2020;583:830–833.
10. Li Y, Zhou W, Yang L, You R. Physiological and pathological regulation of ACE2, the SARS-CoV-2 receptor. *Pharmacol Res* 2020;157:104833.
11. Wan Y, Shang J, Graham R, Baric RS, Li F. Receptor recognition by the novel coronavirus from Wuhan: an analysis based on decade-long structural studies of SARS coronavirus. *J Virol* 2020;94:e00733-19.
12. Hoffmann M, Kleine-Weber H, Schroeder S, Kruger N, Herrler T, Erichsen S, *et al*. SARS-CoV-2 cell entry depends on ACE2 and TMPRSS2 and Is blocked by a clinically proven protease inhibitor. *Cell* 2020;181:271–280, e8.
13. Zhou F, Yu T, Du R, Fan G, Liu Y, Liu Z, *et al*. Clinical course and risk factors for mortality of adult inpatients with COVID-19 in Wuhan, China: a retrospective cohort study. *Lancet* 2020;395:1054–1062.
14. Walls AC, Park YJ, Tortorici MA, Wall A, McGuire AT, Veesler D. Structure, function, and antigenicity of the SARS-CoV-2 spike glycoprotein. *Cell* 2020;181:281–292, e6.
15. Tian X, Li C, Huang A, Xia S, Lu S, Shi Z, *et al*. Potent binding of 2019 novel coronavirus spike protein by a SARS coronavirus-specific human monoclonal antibody. *Emerg Microbes Infect* 2020;9: 382–385.
16. Lan J, Ge J, Yu J, Shan S, Zhou H, Fan S, *et al*. Structure of the SARS-CoV-2 spike receptor-binding domain bound to the ACE2 receptor. *Nature* 2020;581:215–220.
17. Wrapp D, Wang N, Corbett KS, Goldsmith JA, Hsieh CL, Abiona O, *et al*. Cryo-EM structure of the 2019-nCoV spike in the prefusion conformation. *Science* 2020;367:1260–1263.
18. Sun SH, Chen Q, Gu HJ, Yang G, Wang YX, Huang XY, *et al*. A mouse model of SARS-CoV-2 infection and pathogenesis. *Cell Host Microbe* 2020;28:124–133, e4.
19. Wölfel R, Corman VM, Guggemos W, Seilmaier M, Zange S, Müller MA, *et al*. Virological assessment of hospitalized patients with COVID-2019. *Nature* 2020;581:465–469.
20. Farkash EA, Wilson AM, Jentzen JM. Ultrastructural evidence for direct renal infection with SARS-CoV-2. *J Am Soc Nephrol* 2020;31: 1683–1687.
21. Renteria AE, Endam Mfuna L, Adam D, Filali-Mouhim A, Maniakas A, Rousseau S, *et al*. Azithromycin downregulates gene expression of IL-1β and pathways involving TMPRSS2 and TMPRSS11D required by SARS-CoV-2. *Am J Respir Cell Mol Biol* 2020;63:707–709.
22. Ota C, Ng-Blichfeldt JP, Korfei M, Alsafadi HN, Lehmann M, Skronska-Wasek W, *et al*. Dynamic expression of HOPX in alveolar epithelial cells reflects injury and repair during the progression of pulmonary fibrosis. *Sci Rep* 2018;8:12983.
23. Cheung WK, Zhao M, Liu Z, Stevens LE, Cao PD, Fang JE, *et al*. Control of alveolar differentiation by the lineage transcription factors GATA6 and HOPX inhibits lung adenocarcinoma metastasis. *Cancer Cell* 2013;23:725–738.
24. Liao M, Liu Y, Yuan J, Wen Y, Xu G, Zhao J, *et al*. Single-cell landscape of bronchoalveolar immune cells in patients with COVID-19. *Nat Med* 2020;26:842–844.
25. Juno JA, Tan HX, Lee WS, Reynaldi A, Kelly HG, Wragg K, *et al*. Humoral and circulating follicular helper T cell responses in recovered patients with COVID-19. *Nat Med* 2020;26:1428–1434.
26. He R, Lu Z, Zhang L, Fan T, Xiong R, Shen X, *et al*. The clinical course and its correlated immune status in COVID-19 pneumonia. *J Clin Virol* 2020;127:104361.
27. Hassan AO, Case JB, Winkler ES, Thackray LB, Kafai NM, Bailey AL, *et al*. SARS-CoV-2 infection model im dice demonstrates protection by neutralizing antibodies. *Cell* 2020;182:744–753, e4.
28. Sun J, Zhuang Z, Zheng J, Li K, Wong RL, Liu D, *et al*. Generation of a broadly useful model for COVID-19 pathogenesis, vaccination, and treatment. *Cell* 2020;182:734–743, e5.
29. Ackermann M, Verleden SE, Kuehnel M, Haverich A, Welte T, Laenger F, *et al*. Pulmonary vascular endothelialitis, thrombosis, and angiogenesis in covid-19. *N Engl J Med* 2020;383:120–128.
30. Thevarajan I, Nguyen THO, Koutsakos M, Druce J, Caly L, van de Sandt CE, *et al*. Breadth of concomitant immune responses prior to patient recovery: a case report of non-severe COVID-19. *Nat Med* 2020;26: 453–455.

31. Meckiff BJ, Ramirez-Suastegui C, Fajardo V, Chee SJ, Kusnadi A, Simon H, *et al*. Single-cell transcriptomic analysis of SARS-CoV-2 reactive CD4(+) T cells [preprint]. bioRxiv; [accessed 2020 Jun 12]. Available from: https://www.biorxiv.org/content/10.1101/2020.06. 12.148916v1.

32. Liu F, Dai S, Feng D, Qin Z, Peng X, Sakamuri SSVP, *et al*. Distinct fate, dynamics and niches of renal macrophages of bone marrow or embryonic origins. *Nat Commun* 2020;11:2280.

33. Hu W, Ferris SP, Tweten RK, Wu G, Radaeva S, Gao B, *et al*. Rapid conditional targeted ablation of cells expressing human CD59 in transgenic mice by intermedilysin. *Nat Med* 2008;14: 98–103.

34. Feng D, Dai S, Liu F, Ohtake Y, Zhou Z, Wang H, *et al*. Cre-inducible human CD59 mediates rapid cell ablation after intermedilysin administration. *J Clin Invest* 2016;126:2321–2333.

35. Liu F, Dai S, Feng D, Peng X, Qin Z, Kearns AC, *et al*. Versatile cell ablation tools and their applications to study loss of cell functions. *Cell Mol Life Sci* 2019;76:4725–4743.

36. Dai S, Liu F, Qin Z, Zhang J, Chen J, Ding WX, *et al*. Kupffer cells promote T-cell hepatitis by producing CXCL10 and limiting liver sinusoidal endothelial cell permeability. *Theranostics* 2020;10: 7163–7177.

37. Subbarao K, Roberts A. Is there an ideal animal model for SARS? *Trends Microbiol* 2006;14:299–303.